Polytechnic Journal

Polytechnic Journal

Volume 15 | Issue 1 Article 5

Numerical Analysis of the Flexural Strength and Ductility of RC Beams Strengthened with Steel-Reinforced Grout (SRG) Composites

Kamaran S. Ismail

Civil Engineering Department, Erbil Technical Engineering College, Erbil Polytechnic University, Erbil, Kurdistan-Region, Iraq, kamaran.ismail@epu.edu.iq

How to Cite This Article

Ismail, Kamaran S. (2025) "Numerical Analysis of the Flexural Strength and Ductility of RC Beams Strengthened with Steel-Reinforced Grout (SRG) Composites," *Polytechnic Journal*: Vol. 15: Iss. 1, Article 5.
DOI: https://doi.org/10.59341/2707-7799.1854

Numerical Analysis of the Flexural Strength and Ductility of RC Beams Strengthened with Steel-Reinforced Grout (SRG) Composites

Data Availability Statement

The data supporting the findings of this study are publicly available and are included within this published article.

ORIGINAL ARTICLE

Numerical Analysis of the Flexural Strength and Ductility of RC Beams Strengthened with Steel-Reinforced Grout (SRG) Composites

Kamaran S. Ismail

Civil Engineering Department, Erbil Technical Engineering College, Erbil Polytechnic University, Erbil, Kurdistan-Region, Iraq

Abstract

This research examines the flexural behavior and ductility of reinforced concrete beams strengthened with steel-reinforced grout (SRG) composites using a numerical modeling approach. Experimental results from nine SRG-strengthened beams, as reported in the literature, were used to validate the model. The validated model was applied in a comprehensive parametric study to explore how the number of SRG layers, flexural reinforcement ratio, and SRG end anchorage affect the flexural performance and ductility of the beams. The findings show that SRG provides an effective solution for strengthening under-reinforced beams, notably improving their load-carrying capacity and mid-span deflection. However, the technique has little effect on beams that already possess adequate reinforcement. To further analyze SRG's impact on the flexural capacity of RC beams, the numerical results were compared to predicted strength values obtained through the section analysis method. Both the ACI 549-4R13 and ACI 440.2R-08 design strain models were incorporated in the analysis. The findings revealed that, although ACI 440.2R-08 design strain model was not initially developed for SRG, it yielded more accurate results than ACI 549-4R13. As a result, until more design guidelines are developed, it is recommended to use the ACI 440.2R-08 provisions for predicting the flexural capacity of SRG-strengthened RC beams.

Keywords: Flexural behavior, Ductility, Steel-reinforced grout, Numerical analysis, Section analysis

1. Introduction

RC structures deteriorate over time because of factors like reinforcement corrosion, overloading, and poor design, creating an urgent demand for robust retrofitting strategies. Over the past three decades, research has explored the incorporation of externally bonded fiber-reinforced polymer (FRP) composites in various configurations to enhance the flexural and shear capacity of RC elements. FRP materials offer several significant benefits, such as their lightweight nature, ease of installation, and excellent corrosion resistance. Despite the proven application and durability benefits of epoxy, epoxy−FRP systems have certain limitations, including poor adhesion to damp surfaces, low fire resistance, reduced effectiveness at high temperatures, toxicity, irreversibility, and lack of vapor permeability [1−7].

Another approach to enhancing structural performance is the incorporation of shape memory alloys (SMAs) as a reinforcement technique. While SMAs offer several advantages, one notable limitation is their relatively low elastic modulus, particularly in nickel (Ni) and copper (Cu)-based variants [8]. This characteristic can limit their effectiveness in applications requiring high stiffness. In contrast, iron (Fe)-based SMAs exhibit a higher initial elastic modulus, making them a more suitable option in certain cases. However, upon activation and subsequent loading, a reduction in elastic modulus occurs, which can influence their long-term mechanical behavior [9]. This phenomenon must be carefully evaluated when leveraging the shape memory effect of Fe-based SMAs for structural reinforcement.

In response to these disadvantages, Fabric Reinforced Cementitious Matrices (FRCM) composites

Received 6 February 2025; accepted 31 March 2025.
Available online 16 May 2025

E-mail address: kamaran.ismail@epu.edu.iq.

https://doi.org/10.59341/2707-7799.1854

have been adopted to replace FRP systems, using inorganic materials such as grout for impregnation instead of organic counterparts. Despite being less efficient in mechanical bonding with fibers than organic matrices, inorganic matrices offer key advantages, such as ease of use, compatibility with substrates, better thermal performance, and cost efficiency [1,6,7,10–15]. The scientific community has recently focused on steel textiles due to their relatively low cost compared to other fiber textiles and their favorable mechanical properties. When used to reinforce composites, this approach is referred to as Steel Reinforced Grout (SRG) with inorganic matrices.

Steel-based textiles are embedded in a grout matrix to form Steel-Reinforced Grout (SRG) composites. The textiles comprise micro-strands of high-tensile steel, arranged into twisted cords to optimize matrix impregnation. These cords are systematically aligned to create a unidirectional fabric (Fig. 1). A bidirectional glass fabric, affixed with strong adhesives, regulates the cord spacing. The design of SRG textiles can be adjusted by varying the number and arrangement of steel wires, modifying both the mechanical response of the textile and the degree of mortar permeation through the mesh openings. Furthermore, the internal reinforcement capacity of SRG depends on the ability of the matrix to effectively transfer stresses to the steel wires. The textile's density is defined by the number of cords per inch, commonly 4 or 8 cords/inch.

The commercial adoption of SRG composites has, until recently, been predominantly applied to the reinforcement of masonry structures, including arches and stone walls. In recent years, their use in reinforced concrete components has gained attention, with several research institutions investigating their suitability for applications ranging from external strengthening in rehabilitation projects to the fabrication of precast elements. Researchers have studied the SRG strengthening system through experimental testing on beams subjected to flexural and shear strengthening [1,3–7,15]. While these studies provide meaningful data, the limited scope of testing highlights the need for further research. In particular, a deeper understanding of bond interactions at the concrete-SRG and steel fabric-mortar interfaces is required, along with an assessment of the accuracy and applicability of existing code provisions for predicting the strength of SRG-strengthened RC beams.

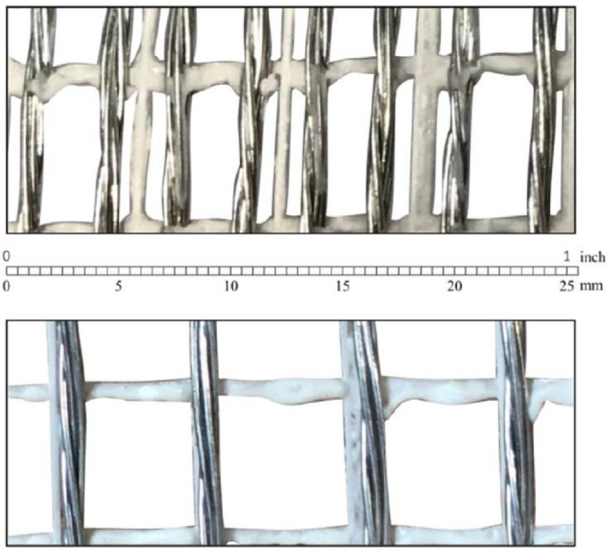

Fig. 1. Steel textiles of density (Top 8 cords/inch and Bottom) 4 cords/inch.

The main objective of this research is to analyze the impact of different SRG composite layers on the flexural behavior and ductility of RC beams. It also examines how stress transfer mechanisms are influenced by textile layer density. The findings are then utilized to develop practical design guidelines for optimizing SRG system efficiency and are compared with the latest standards for applying SRG composites in RC beam strengthening. A numerical approach is used in this study, starting with model validation against experimental data from published research. Once validated, a computational parametric study is conducted to examine the influence of key design variables on the performance of strengthened beams. These variables include the proportion of steel textile to internal reinforcement, the number of applied textile layers, and the role of the anchorage system in enhancing beam performance.

2. Numerical analysis

2.1. Model description

Numerical modeling is performed using ABAQUS, a general finite element program, and the results of nine RC beams found in the literature [6,7] are examined to validate the model. A summary of the beam details can be found in Table 1. Prescribed displacements at designated loading points are used to apply the load, enabling the evaluation of failure load and post-peak performance. Concrete is modeled with 8-noded linear brick elements (C3D8R), while the steel bars are modeled as 2-noded linear beam elements (B31). Unlike truss elements, which can only resist axial forces such as compression or tension, beam elements can accommodate both axial and bending forces. This

Table 1. Summary of beams used for model validation.

NO.	Reference	Beam ID	Length (mm)	Height (mm)	Width (mm)	SRG Layers	SRG Design thickness (mm)
1	Larrinaga et al.	R1	1350	150	150	N/A	N/A
2	2020 [6]	LS1	1350	150	150	1	0.075
3		LS2	1350	150	150	2	0.075
4		LS3	1350	150	150	3	0.075
5		MS1	1350	150	150	1	0.225
6	Alotaibi 2021 [7]	B-REF	2300	250	150	N/A	N/A
7		B-S4-1	2300	250	150	1	0.084
8		B-S4-2	2300	250	150	2	0.084
9		B-S8-2	2300	250	150	1	0.169

allows them to better simulate the actual behavior of reinforcement and capture effects like dowel action as a shear stress transfer mechanism. The bars are embedded within the concrete to maintain a perfect bonding between the concrete and the reinforcement.

Concrete behavior is simulated using the damaged plasticity model from the ABAQUS material library. Saenz's model [16] is employed to simulate the compressive stress–strain behavior of concrete (EQ (1)), while the tensile stress–strain behavior is modeled using the pre- and post-cracking equations proposed by Belarbi and Hsu [17] (EQ (2) and EQ (3), respectively).

$$\sigma_c = \frac{E_c \varepsilon_c}{1 + (R + R_E - 2)\left(\frac{\varepsilon_c}{\varepsilon_o}\right) - (2R - 1)\left(\frac{\varepsilon_c}{\varepsilon_o}\right)^2 + R\left(\frac{\varepsilon_c}{\varepsilon_o}\right)^3} \quad \text{(Eq.1)}$$

where

$$R = \frac{R_E(R_\sigma - 1)}{(R_\varepsilon - 1)^2} - \frac{1}{R_\varepsilon}, R_E = \frac{E_c}{E_o}, E_o = \frac{f_{ck}}{\varepsilon_o},$$

As per the work of Hu and Schnobrich [18] $R_\sigma = 4$ and $R_\varepsilon = 4$ can be utilized. The value of ε_o, which corresponds to the concrete strain corresponding to the peak stress (f_{ck}), is typically taken as 0.002.

$$\sigma_t = E_c \varepsilon_t;\ \varepsilon_t \le \varepsilon_{cr} \quad \text{(Eq.2)}$$

$$\sigma_t = f_{tk}\left(\frac{\varepsilon_{cr}}{\varepsilon_t}\right)^{0.4};\ \varepsilon_t > \varepsilon_{cr} \quad \text{(Eq.3)}$$

where f_{tk} is the cracking stress of the concrete and $\varepsilon_{cr} = f_{tk}/E_c$; E_c is the modulus of elasticity of the concrete and, in this study, it has been calculated based on ACI 318-19 [19].

An elastic-perfectly plastic stress–strain model was used to simulate the behavior of reinforcing steel in tension and compression, and the SRG composite was represented as a homogeneous elastic material with an elastic modulus of 200 GPa and a Poisson's ratio of 0.3, until failure. The interaction between SRG and concrete was represented by a cohesive surface interface. Relative displacements were described using the traction-separation approach, which features a bilinear response with an initial elastic behavior followed by a softening phase to capture damage evolution. The model considers two failure modes: one governed by normal stresses and the other by shear stresses as shown in Fig. 2.

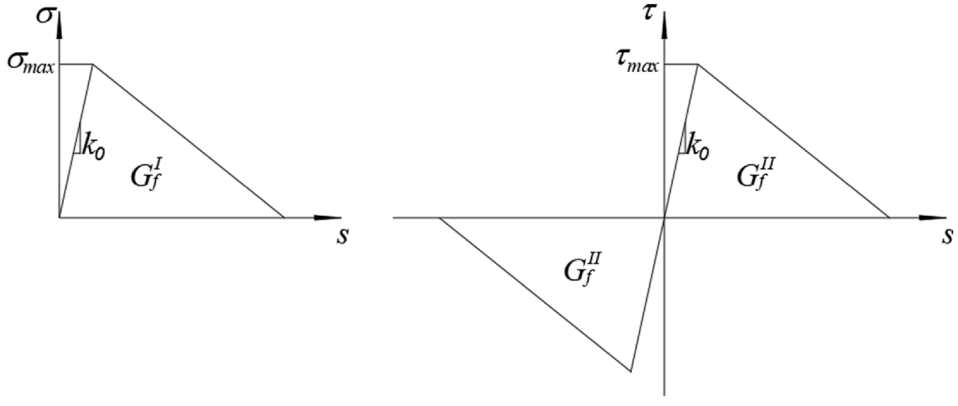

Fig. 2. Traction-separation approach.

Due to the lack of comprehensive studies on the mechanism of stress transmission at the SRG-concrete interface, the bilinear bond-slip law introduced by Lu et al. [20] is employed in this research. Although this bond-slip model was initially formulated for FRP composites, it can also be applied to SRG systems. This is because FRP and SRG demonstrate comparable load-slip responses, making it feasible to use the same bond-slip law to describe the bond behavior at the SRG-concrete interface. The bond-slip behavior is primarily defined by three parameters: the initial stiffness (k_0), which controls the elastic response of the interface; the peak shear stress (τ_{max}), which indicates the maximum bond strength before failure initiates; and the fracture energy (G_f), which characterizes the energy required for complete bond failure. The values of these parameters, as derived from the experimental results [21]. The resulting bilinear model, shown in Fig. 3, is outlined in the subsequent equations:

$$\tau = \tau_{max}\frac{s}{s_o} \quad if\ s \le s_o \tag{Eq.4}$$

$$\tau = \tau_{max}\frac{s_f - s}{s_f - s} \quad if\ s_o \le s \le s_f \tag{Eq.5}$$

$$\tau = 0 \quad if\ s \ge s_f \tag{Eq.6}$$

where

$$s_f = \frac{2G_f}{\tau_{max}} \tag{Eq.7}$$

$$\tau_{max} = 1.5\beta_w f_{tk} \tag{Eq.8}$$

$$s_o = 0.0095\beta_w f_{tk} + s_e \tag{Eq.9}$$

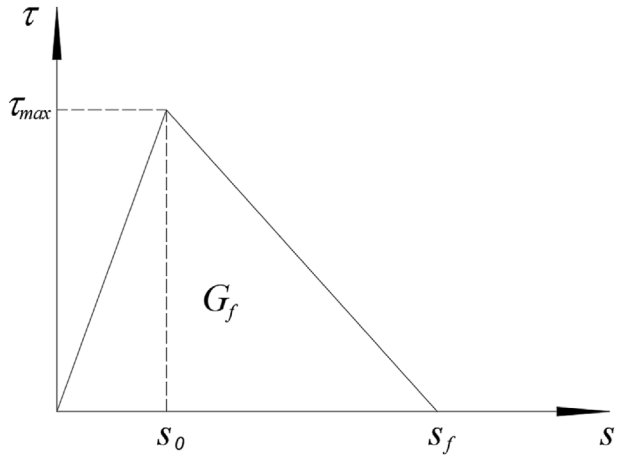

Fig. 3. Bond-slip model.

$$s_e = \frac{\tau_{max}}{k_0} \tag{Eq.10}$$

$$\beta_w = \sqrt{\frac{2.25 - b_f/b_c}{1.25 + b_f/b_c}} \tag{Eq.11}$$

$$G_f = 0.308\beta_w^2\sqrt{f_{tk}} \tag{Eq.12}$$

The current research identified k_0 as 78N/mm^3, which provided the best match with experimental data. The tensile strength, f_{tk} was taken as 0.62 $\sqrt{f_c}$ based on the modulus of rupture formula specified in the ACI 318-19 code. The parameters b_f and b_c refer to the widths of the SRG composite and the cross-section of the beam, respectively.

2.2. Model validation

Due to the inherent challenges of modeling concrete's mechanical properties, simulating concrete structures using finite element methods remains a demanding process. Reliable validation with experimental results is a key step to verify the model's predictive accuracy and dependability. Experimental data from nine RC beams available in the literature were used to validate the proposed numerical model, verifying its accuracy in simulating the structural response of RC beams strengthened with SRG composites.

The numerically predicted load-deflection responses, compared with experimental results of nine RC beams found in the literature [6,7], are shown in Figs. 4 and 5. The results demonstrate a high level of consistency between numerical and experimental data, providing accurate predictions of the beams' behavior throughout the loading history. Once flexural cracking occurs, the experimental load-deflection behavior, in some of the beams, is slightly less stiff than the numerical predictions. This variation is primarily attributed to the smeared stress–strain representation in the numerical model, which cannot fully capture the localized effects of tension stiffening, strain variation, and stiffness degradation caused by debonding and reinforcement slip at crack locations. Fig. 6 experimental and finite element SRG debonding for beam MS1 tested by Larrinaga et al. [6] and Fig. 7 shows the finite element predicted crack pattern against experimental crack pattern for beam at ultimate load for beam B-S4-2 tested by Alotaibi [7]. Generally the developed finite element model demonstrates good accuracy in modeling the behavior of RC beams strengthened with SRG composites, making it suitable for further studies

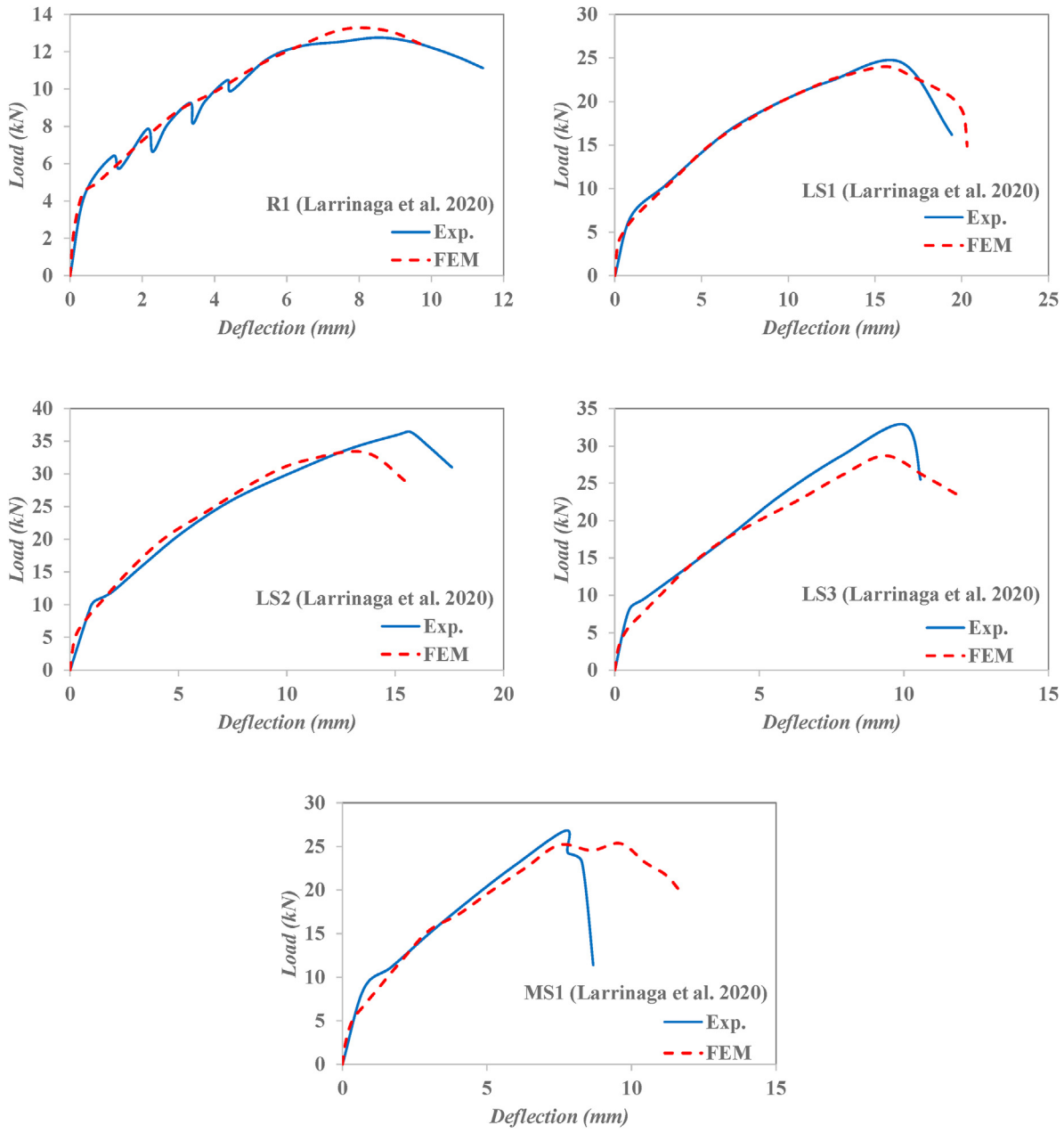

Fig. 4. Experimental vs predicted load-deflection curves for beams tested by Larrinaga et al. [6].

on the effects of various design parameters on the behavior and strength of comparable structural elements.

3. Parametric investigation

A parametric study was conducted to assess the influence of different design parameters and strengthening techniques on the strength and serviceability of RC beams reinforced with SRG composites. The design parameters evaluated include the ratio of internal reinforcement, the number of SRG layers, and the anchorage of SRG at the beam ends. The considered beams are full-scale specimens with a 7.0 m span, 600 mm height, and 400 mm width. The concrete compressive strength of the beams is 21 MPa. Detailed specifications of the specimens used in this parametric study are provided in Table 2 and the beam details are shown in Fig. 8. Four-point bending tests were conducted on the beams, with loads applied through controlled displacements at the loading points to assess failure loads and post-peak behavior. The SRG systems in this study match the

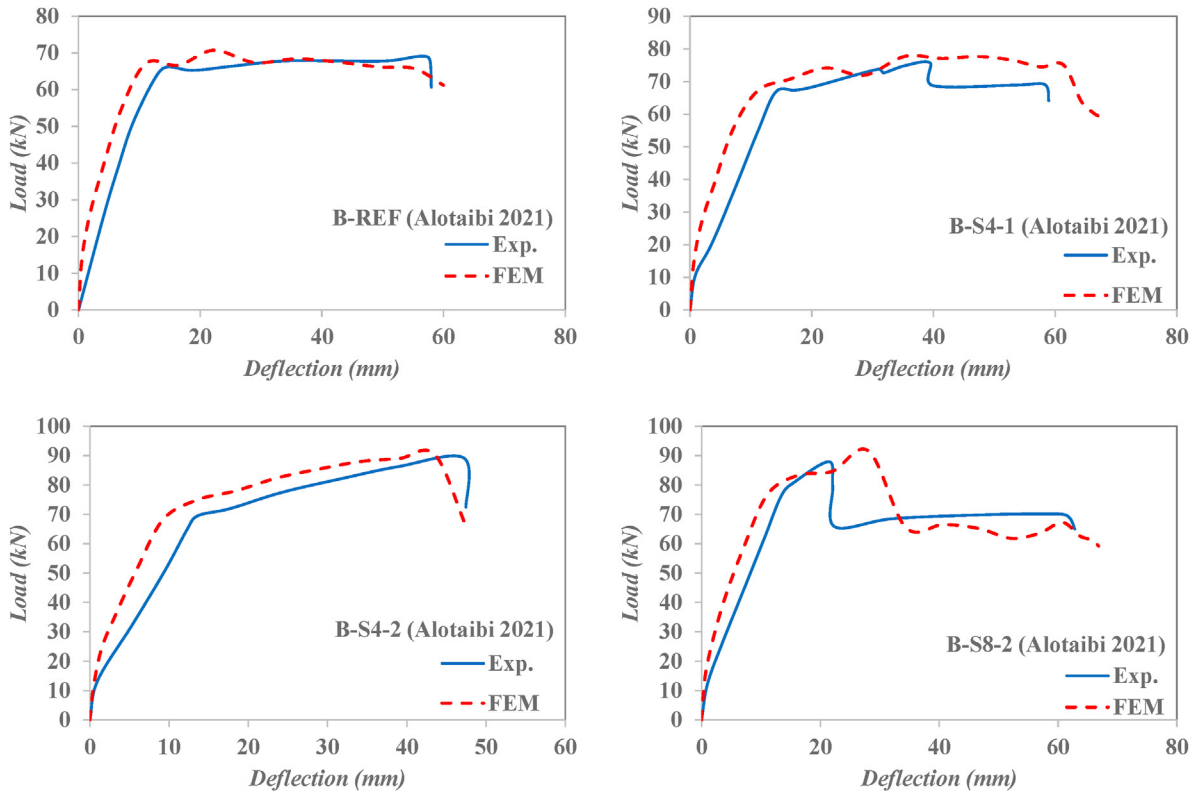

Fig. 5. Experimental vs predicted load-deflection curves for beams tested by Alotaibi [7].

specifications of commercially popular SRGs, manufactured using textile fabrics incorporating high-strength galvanized steel cords with twisted microwires. These systems have a design thickness of 0.169 mm, modulus of elasticity of 200 GPa, an ultimate strength of 3200 MPa, The ultimate tensile strain of the of 0.015 with standard deviation (STD) of 0.001. The matrix is assumed to exhibit

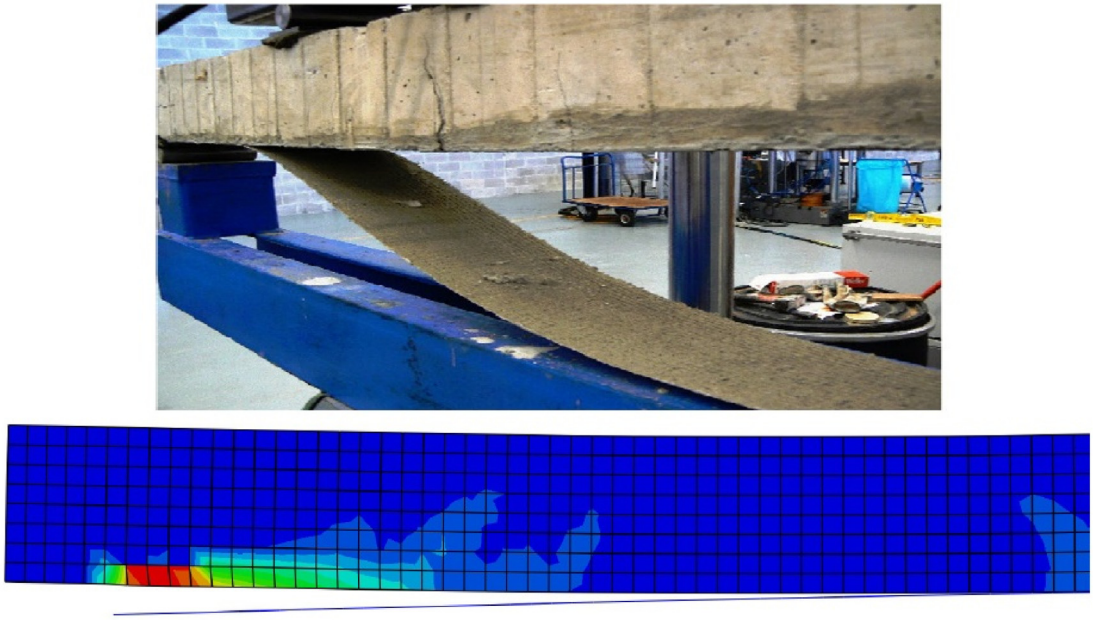

Fig. 6. Experimental vs finite element SRG debonding for beam MS1 tested by Larrinaga et al. [6].

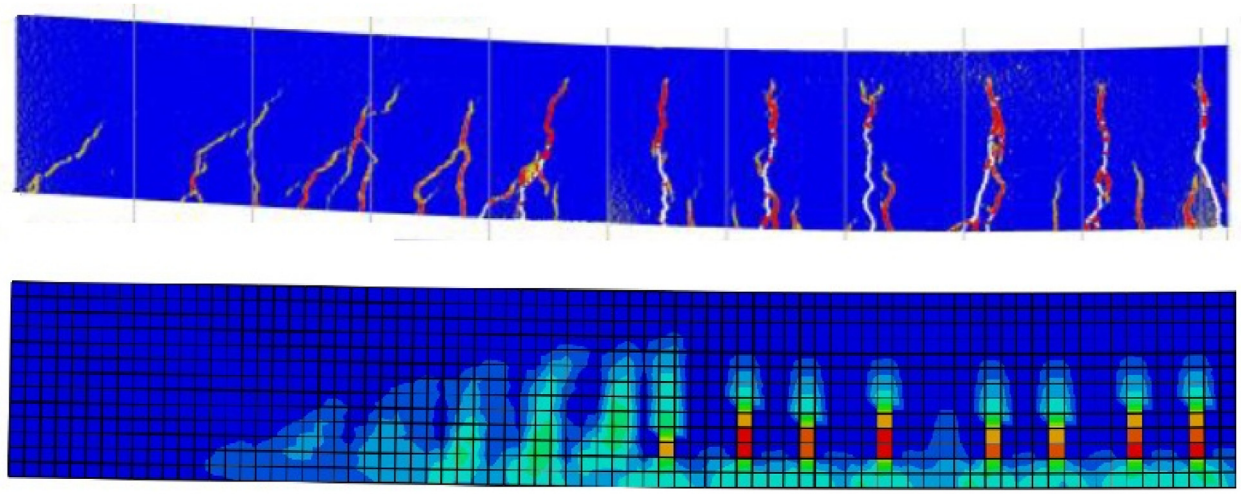

Fig. 7. Experimental vs finite element crack pattern at ultimate load for beam B-S4-2 tested by Alotaibi [7].

Table 2. Details of the beams used for the parametric study.

NO.	Beam ID	ρ_s	SRG Layers	ρ_{SRG}	Anchorage
1	B-R4-S0	0.00369	0	0	……
2	B-R6-S0	0.00554	0	0	……
3	B-R8-S0	0.00738	0	0	……
4	B-R4-S1	0.00369	1	0.0002817	……
5	B-R6-S1	0.00554	1	0.0002817	……
6	B-R8-S1	0.00738	1	0.0002817	……
7	B-R4-S2	0.00369	2	0.0005633	……
8	B-R6-S2	0.00554	2	0.0005633	……
9	B-R8-S2	0.00738	2	0.0005633	……
10	B-R4-S3	0.00369	3	0.000845	……
11	B-R6-S3	0.00554	3	0.000845	……
12	B-R8-S3	0.00738	3	0.000845	……
13	B-R4-S1-A	0.00369	1	0.0002817	Both Ends
14	B-R6-S1-A	0.00554	1	0.0002817	Both Ends
15	B-R8-S1-A	0.00738	1	0.0002817	Both Ends
16	B-R4-S2-A	0.00369	2	0.0005633	Both Ends
17	B-R6-S2-A	0.00554	2	0.0005633	Both Ends
18	B-R8-S2-A	0.00738	2	0.0005633	Both Ends
19	B-R4-S3-A	0.00369	3	0.000845	Both Ends
20	B-R6-S3-A	0.00554	3	0.000845	Both Ends
21	B-R8-S3-A	0.00738	3	0.000845	Both Ends

compressive and tensile strengths of 30 MPa and 3.0 MPa, respectively.

3.1. Load-deflection responses

The load-deflection characteristics at midspan for beams from the parametric analysis are displayed in Fig. 9, Figs. 10 and 11. The curves are arranged according to the main reinforcement ratio and the anchorage of the SRG system. The load-deflection behavior of the beams can be divided into three distinct phases. Phase 1, which ends at crack formation, represents the elastic response. Phase 2 continues up to a sharp change in the curve's slope, signifying semi-linear behavior that ends when the tension reinforcement reaches its yield point. Phase 3 is characterized by a significant reduction in stiffness, with deflection increasing notably under small load increments until the beam fails. The progression of the three phases can vary based on

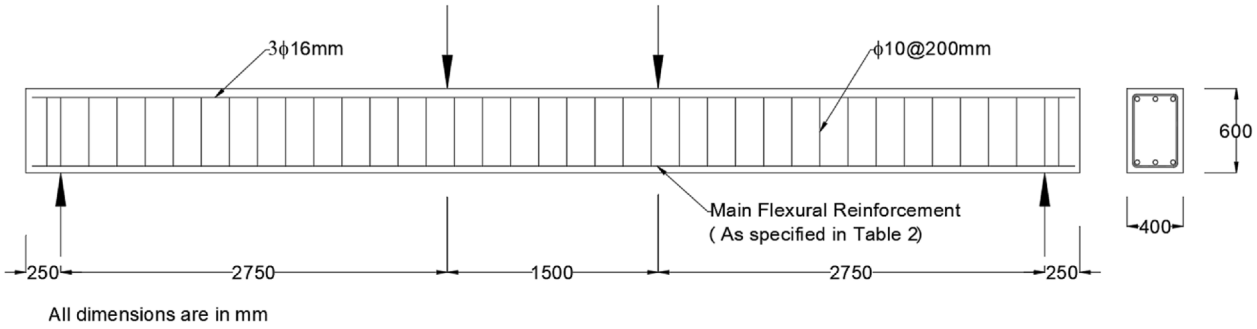

Fig. 8. Details of the beams used for the parametric study.

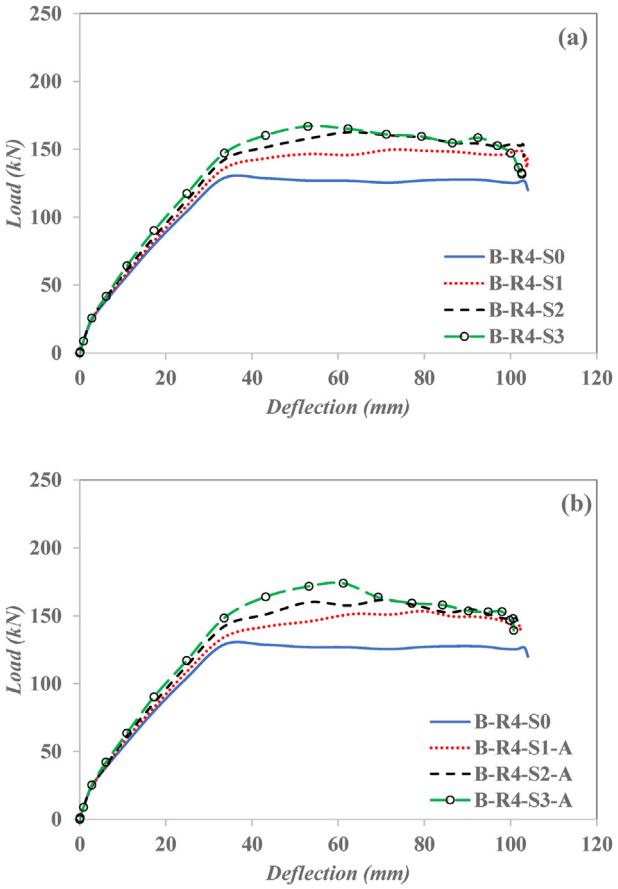

Fig. 9. Load-Deflection curve for the beams with reinforcement ratio of 0.00369 a) beams without end anchorage and b) beams with end anchorage.

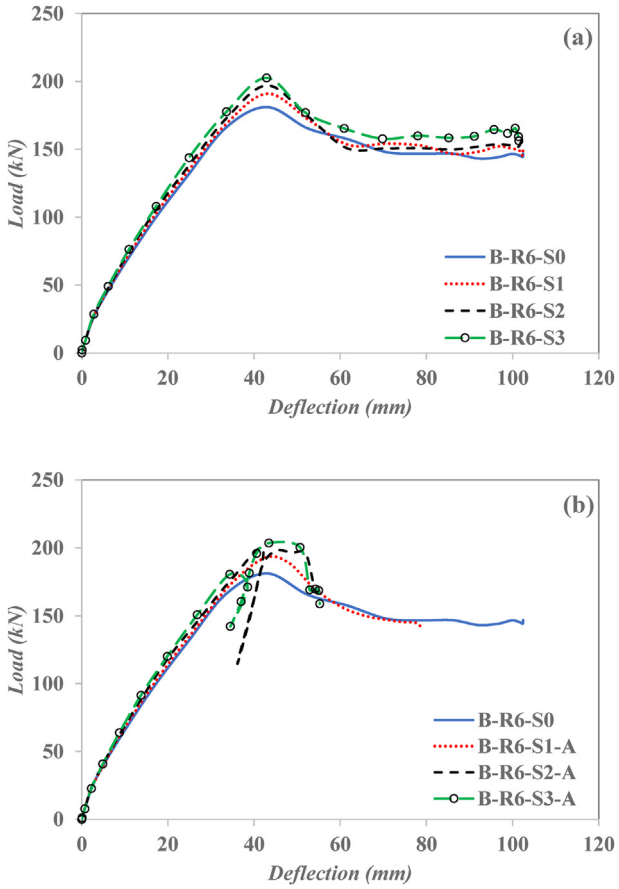

Fig. 10. Load-Deflection curve for the beams with reinforcement ratio of 0.00554 a) beams without end anchorage and b) beams with end anchorage.

the main reinforcement ratio and the number of SRG composite layers.

3.2. Results and discussion

The effect of essential design parameters on the flexural strengthening efficiency of SRG beams is investigated in this section. The effect of varying the number of SRG composite layers on beam strength and midspan deflection is shown in Fig. 12. In the figure, the beams are grouped and labeled based on their internal reinforcement ratio. For example, R4 designates beams with four 16 mm bars, which corresponds to a reinforcement ratio of 0.369 %, while A indicates the use of SRG composite anchorage. It can be seen in the figure that strengthening with one SRG composite layer improves the beam's strength by roughly 16 %, though this effect is less pronounced in beams with a higher internal reinforcement ratio. This occurs because, in beams with lower reinforcement, the SRG composite plays a role in stress transfer early during loading since the internal reinforcement has limited capacity. For beams with higher reinforcement, the internal reinforcement accommodates the internal moment, and the SRG's contribution occurs at later stages. At this point, the interface between the SRG and the beam deteriorates, causing debonding and eventual failure.

The second design parameter investigated is the anchorage of SRG composites at the beam ends. Fig. 12 shows these beams in groups marked with (A). It is evident from the figure that end anchorage has little effect on the beam strength. However, a 10 % increase in midspan deflection is observed for beams with a reinforcement ratio of 0.369 % (R4 and R4-A). This is largely due to the fact that the SRG composites' effectiveness in enhancing beam strength and ductility is controlled by intermediate crack-induced debonding rather than end debonding. Fig. 13 illustrates the intermediate crack (shown in gray), which triggers this type of debonding and disrupts stress transfer between the SRG composites and the beam interface.

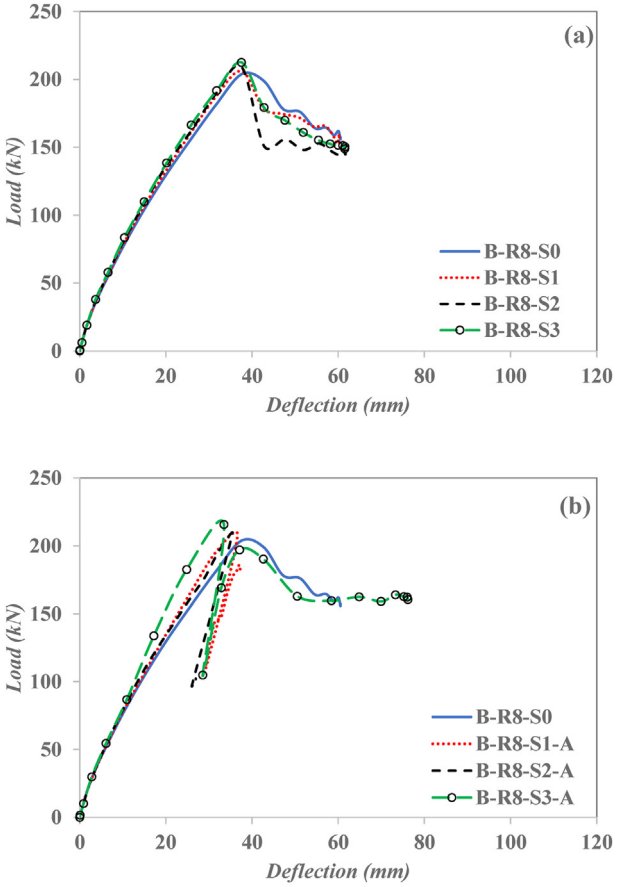

Fig. 11. Load-Deflection curve for the beams with reinforcement ratio of 0.00738 a) beams without end anchorage and b) beams with end anchorage.

To assess the effect of SRG layers on RC beam behavior, the displacement ductility index is determined. This index is the ratio of displacement at the yielding of the flexural reinforcement to the failure deflection, with the results displayed in Fig. 14. The figure clearly shows that the ductility of beams with a flexural reinforcement ratio of 0.369 %, which closely matches the minimum reinforcement ratio specified in the ACI 318-19 code, is improved by applying a single layer of SRG composite, with additional enhancement observed when SRG end anchorages are included. However, as the reinforcement ratio increases, the effect of SRG strengthening on beam ductility becomes negligible.

4. Analytical model

Since the beams under investigation are slender, the section analysis method, which assumes that a plane section before bending remains plane after bending, can be applied with high accuracy. This method is straightforward for unstrengthened beams. However, for beams reinforced with SRG

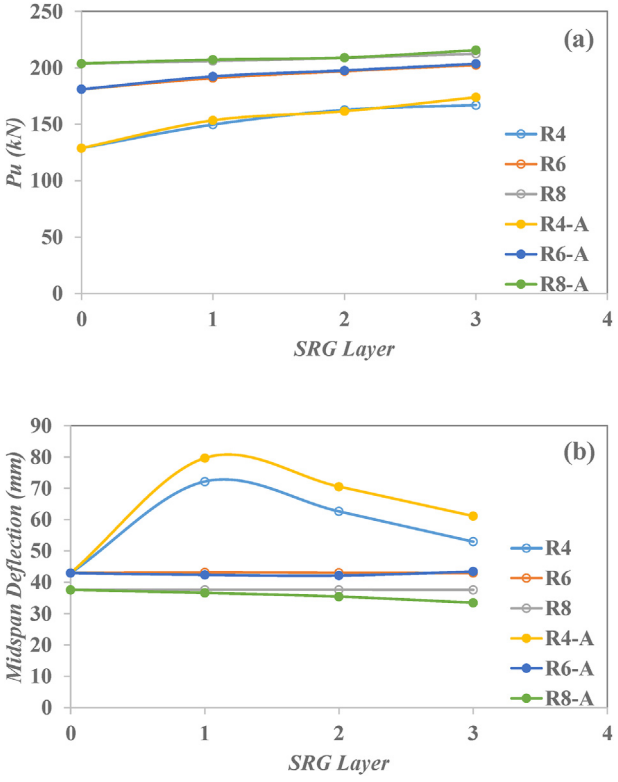

Fig. 12. Effect of SRG layers on a) the capacity of the beams and b) the midspan deflection.

composites on the tension face, additional considerations are necessary due to the risk of debonding. Debonding often prevents the full effectiveness of the external strengthening system, especially in cases with multiple reinforcement layers. Traditional cross-section analysis assumes a perfect bond between the composite and the substrate, thereby neglecting debonding failures. To enhance the accuracy of strength predictions, it is essential to anticipate and incorporate strain at debonding into the method.

The ACI committee report 549-4R13 [22] suggests the following design tensile strain (ε_{fd}) for SRG systems used for strengthening RC members:

$$\varepsilon_{fd} = \varepsilon_{fu} - 1STD \leq 0.0012 \quad \text{(Eq.13)}$$

Where ε_{fu} is the ultimate tensile strain of the SRG and STD is the standard deviation. These values are provided by the manufacturer.

As the number of SRG layers increases, the beam's design tensile strain decreases due to greater composite thickness. However, Eq. (13) does not account for this effect. Therefore, flexural strength predictions based on section analysis using the design strain from ACI 549-4R13 are unreliable, as illustrated in Fig. 15. This inaccuracy can lead to unsafe results, even for beams with a single SRG

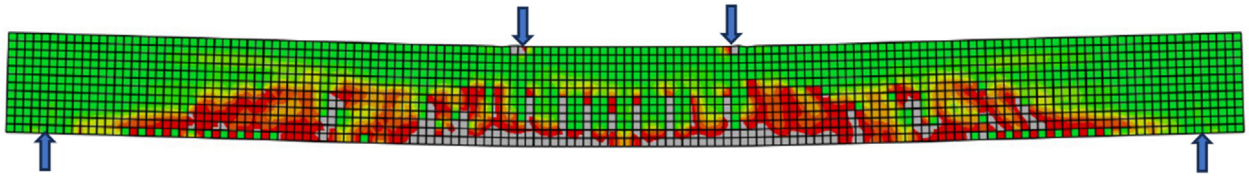

Fig. 13. Intermediate crack-induced debonding for beam LS1 tested by Larrinaga et al. [6].

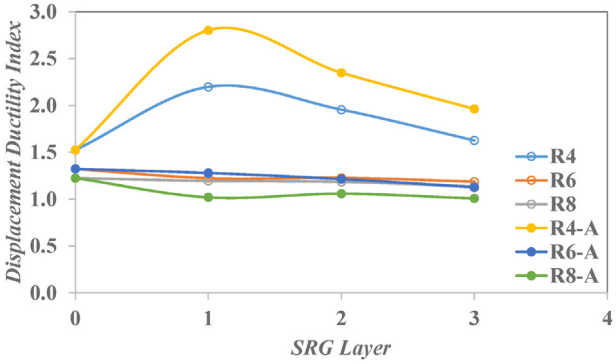

Fig. 14. Effect of SRG layers on the displacement ductility index.

layer, and becomes more pronounced as additional layers are added.

According to the ACI 440.2R-08 guideline [23], which is the design standard for FRP strengthening of reinforced concrete structures, the following formula is used to calculate the design strain (ε_{fd}) of externally bonded FRP reinforcement:

$$\varepsilon_{fd} = 0.41\sqrt{\frac{f'_c}{n.E_f.t_f}} \leq 0.95\varepsilon_{fu} \qquad \text{(Eq.14)}$$

Where n is the number of FRP layers, E_f is the modulus of elasticity, t_f is the thickness of one layer of FRP and ε_{fu} is ultimate strain at failure.

To determine whether Eq. (14) provides improved accuracy over Eq. (13), it is applied in this study to predict the design strain of SRG. Unlike Eq. (13), this equation incorporates additional parameters, including the number of SRG layers, composite thickness, and modulus of elasticity. The corresponding results are shown in Fig. 16. It is obvious

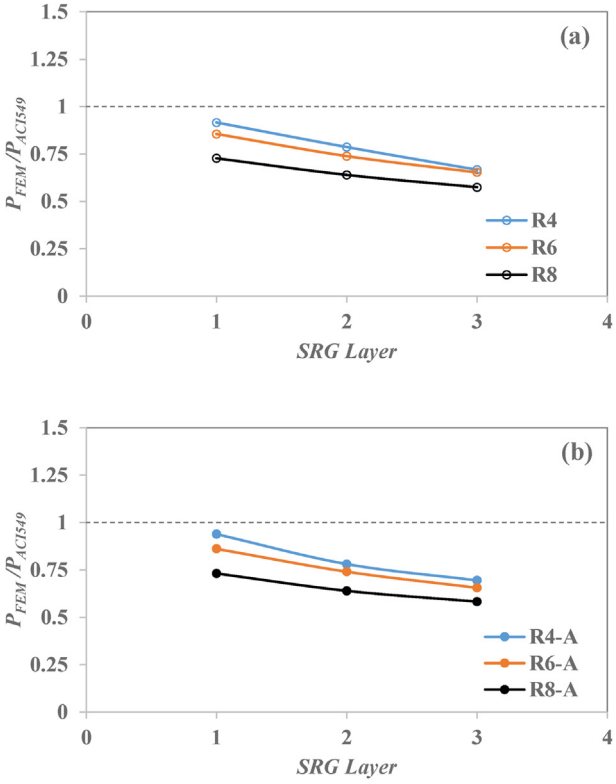

Fig. 15. Section analysis based on ACI committee report 549-4R13 vs FEM, a) beams without end anchorage and b) beams with end anchorage.

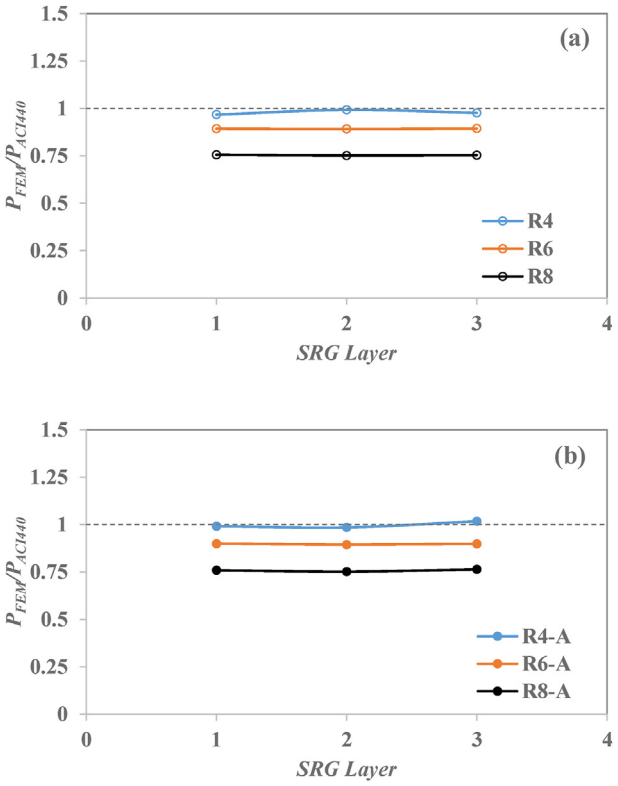

Fig. 16. Section analysis based on ACI 440.2R-08 vs FEM, a) beams without end anchorage and b) beams with end anchorage.

that the results more promising compared to the results of Eq. (13). However, it still can lead to unsafe results especially for beams with proper reinforcement. This is most likely attributed to the fact that the Eq. (14) is originally proposed for beams strengthened with FRP rather than SRG composites.

Until more comprehensive studies are conducted on the flexural performance of SRG-strengthened beams, it is recommended that the design strain of SRG composites be estimated using the ACI 440.2R-08 guideline rather than the ACI 549-4R13 report.

5. Conclusion

The flexural response and ductility of RC beams strengthened with SRG composites were numerically investigated to understand the effect of critical design factors. Based on the outcomes of the FEM analysis and an extensive parametric study, the following conclusions can be made:

- This numerical model reliably predicts the flexural response of RC beams strengthened with SRG composites and is a valuable tool for investigating the effects of various design parameters on their ultimate strength and behavior.
- Strengthening RC beams with one layer of SRG composite can increase their strength by approximately 16 %, but this enhancement is less evident in beams with a higher internal reinforcement ratio.
- The presence of SRG end anchorage has little influence on the strength of the beam. However, it improves midspan deflection by 10 % in beams with a reinforcement ratio of 0.369 % and one SRG composite layer, with no further benefits from additional layers.
- The ductility of beams with a flexural reinforcement ratio of 0.369 %, which closely aligns with the minimum reinforcement ratio specified in the ACI 318-19 code, is enhanced by applying a single SRG composite layer. Additional improvement is observed with the inclusion of SRG end anchorages. However, as the reinforcement ratio increases, the influence of SRG strengthening on ductility becomes negligible.
- Flexural strength predictions using section analysis with the design strain from ACI 549-4R13 may yield highly unsafe results and are not recommended. In contrast, the design strain equation from ACI 440.2R-08 provides more reliable outcomes.
- Additional experimental and analytical studies are required to enhance the understanding of RC beams strengthened with SRG and to refine predictive models for more accurate strength estimation. Key aspects, such as intermediate crack-induced debonding and end anchorage, should be explored experimentally.

Ethics information

The data used in this study contain no personal or sensitive information requiring ethical review.

Author contribution

The author contributed solely to all aspects of the manuscript.

AI usage declaration

The author declare that the content of this work was not generated using AI.

Funding

No specific funding was received for conducting this research.

Conflict of interest

The author declare that there is no conflict of interest.

Acknowledgment

The author gratefully acknowledges the support of Erbil Polytechnic University and all individuals who contributed to the successful completion of this study.

References

[1] Triantafillou TC, Papanicolaou CG. Shear strengthening of reinforced concrete members with textile reinforced mortar (TRM) jackets. Mater Struct 2006;39:93–103. https://doi.org/10.1007/s11527-005-9034-3.

[2] Papanicolaou CG, Triantafillou TC, Karlos K, Papathanasiou M. Textile-reinforced mortar (TRM) versus FRP as strengthening material of URM walls: in-plane cyclic loading. Mater Struct 2007;40:1081–97. https://doi.org/10.1617/s11527-006-9207-8.

[3] D'Ambrisi A, Focacci F. Flexural strengthening of RC beams with cement-based composites. J Compos Construct 2011; 15(5):707–20. https://doi.org/10.1061/(ASCE)CC.1943-5614.000021.

[4] Ombres L. Flexural analysis of reinforced concrete beams strengthened with a cement based high strength composite material. Compos Struct 2011;94(1):143–55. https://doi.org/10.1016/j.compstruct.2011.07.008.

[5] Al-Salloum YA, Elsanadedy HM, Alsayed SH, Iqbal RA. Experimental and numerical study for the shear strengthening of reinforced concrete beams using textile-reinforced mortar. J Compos Construct 2012;16(1):74–90. https://doi.org/10.1061/(ASCE)CC.1943-5614.0000239.

[6] Larrinaga P, Garmendia L, Piñero I, San-José J-T. Flexural strengthening of low-grade reinforced concrete beams with

compatible composite material: Steel Reinforced Grout (SRG). Constr Build Mater 2020;235:117790. https://doi.org/10.1016/j.conbuildmat.2019.117790.
[7] Alotaibi S. Flexural behaviour of RC beams strengthened with multi-layer steel reinforced grout (SRG) composites. University of Sheffield; 2021. p. 30604. oai:etheses.whiterose.ac.uk.
[8] Zareie S, Issa AS, Seethaler RJ, Zabihollah A. Recent advances in the applications of shape memory alloys in civil infrastructures: A review. Structures 2020;27:1535–50. https://doi.org/10.1016/j.istruc.2020.05.058.
[9] Shahverdi M, Michels J, Czaderski C, Motavalli M. Iron-based shape memory alloy strips for strengthening rc members: Material behavior and characterization. Constr Build Mater 2018;173:586–99. https://doi.org/10.1016/j.conbuildmat.2018.04.057.
[10] De Felice G, De Santis S, Garmendia L, Ghiassi B, Larrinaga P, Lourenço PB, et al. Mortar-based systems for externally bonded strengthening of masonry. Mater Struct 2014;47:2021–37. https://doi.org/10.1617/s11527-014-0360-1.
[11] Ascione F, Lamberti M, Napoli A, Realfonzo R. Experimental bond behavior of Steel Reinforced Grout systems for strengthening concrete elements. Constr Build Mater 2020;232:117105. https://doi.org/10.1016/j.conbuildmat.2019.117105.
[12] Banholzer B, Brockmann T, Brameshuber W. Material and bonding characteristics for dimensioning and modelling of textile reinforced concrete (TRC) elements. Mater Struct 2006;39:749–63. https://doi.org/10.1617/s11527-006-9140-x.
[13] Corinaldesi V, Donnini J, Mazzoni G. Experimental study of adhesion between FRCM and masonry support. Key Eng Mater 2014;624:189–96. https://doi.org/10.4028/www.scientific.net/KEM.624.189.
[14] Ascione L, De Felice G, De Santis S. A qualification method for externally bonded Fibre Reinforced Cementitious Matrix (FRCM) strengthening systems. Compos B Eng 2015;78:497–506. https://doi.org/10.1016/j.compositesb.2015.03.079.
[15] Tetta ZC, Triantafillou TC, Bournas DA. On the design of shear-strengthened RC members through the use of textile reinforced mortar overlays. Compos B Eng 2018;147:178–96. https://doi.org/10.1016/j.compositesb.2018.04.008.
[16] Saenz L. Equation for the stress-strain curve of concrete in uniaxial and biaxial compression of concrete. ACI Journal 1965;61(9):1229–35.
[17] Belarbi A, Hsu TT. Constitutive laws of concrete in tension and reinforcing bars stiffened by concrete. Structural Journal 1994;91(4):465–74. https://doi.org/10.14359/4154.
[18] Hu H-T, Schnobrich WC. Constitutive modeling of concrete by using nonassociated plasticity. J Mater Civ Eng 1989;1(4):199–216. https://doi.org/10.1061/(ASCE)0899-1561(1989)1:4(19.
[19] ACI Committee 318. Building code requirements for structural concrete (ACI 318-19): an ACI standard; commentary on building code requirements for structural concrete (ACI 318R-19). American Concrete Institute; 2020. 978-1-64195-086-2.
[20] Lu X, Teng J, Ye L, Jiang J. Bond–slip models for FRP sheets/plates bonded to concrete. Eng Struct 2005;27(6):920–37. https://doi.org/10.1016/j.engstruct.2005.01.014.
[21] Ascione F, Lamberti M, Napoli A, Realfonzo R. Experimental bond behavior of Steel Reinforced Grout systems for strengthening concrete elements. Constr Build Mater 2020;232:117105. https://doi.org/10.1016/j.conbuildmat.2019.117105.
[22] ACI Committee 549. Guide to design and construction of externally bonded fabric- reinforced cementitious matrix (FRCM) systems for repair and strengthening concrete and masonry structures. ACI 549.4R-13. Farmington Hills, MI 48331 U.S.A.: American Concrete Institute; 2013. 9780870318528.
[23] ACI Committee 440. Guide for the design and construction of externally bonded FRP systems for strengthening concrete structures. ACI 440.2R-08. Farmington Hills, MI, USA: American Concrete Institute; 2008. 9780870312854.